

Seismic attenuation structure of the top half of the inner core beneath the northeastern Pacific

R. Iritani,¹ N. Takeuchi,¹ and H. Kawakatsu¹

Received 20 May 2010; revised 27 July 2010; accepted 12 August 2010; published 7 October 2010.

[1] We present a 1-D seismic attenuation model of the top 600 km of the inner core beneath the northeastern Pacific. We employ a waveform inversion method for attenuation parameters based on simulated annealing that enables us to analyze complicated waveforms contaminated by phase overlaps. The method also allows analysis of PKP(DF) in distant ranges where only single core phase is present. The resultant data set is about five times larger compared with our previous study. The inverted model shows a gradual increase of the attenuation from the ICB to 200–250 km depth that coincides with a gradual increase of the P-wave velocity in the same depth range. The attenuation decreases from this depth range, and thus shows a peak around 200–250 km. A possible relation of these observations to the growth process of the inner core in the western hemisphere of the inner core is discussed. **Citation:** Iritani, R., N. Takeuchi, and H. Kawakatsu (2010), Seismic attenuation structure of the top half of the inner core beneath the northeastern Pacific, *Geophys. Res. Lett.*, 37, L19303, doi:10.1029/2010GL044053.

1. Introduction

[2] The seismic attenuation structure of the inner core has been studied extensively because it provides constraints on the physical state and properties of the inner core. The existing models, however, apparently disagree. For example, *Doornbos* [1974] analyzed core phases from European stations recording events in the Fiji-Tonga region and suggested the largest attenuation is at the top of the inner core and gradually decreases with depth. In contrast, *Kazama et al.* [2008] analyzed data from stations in Japan recording events in South America, and suggested the largest attenuation occurs at about 200 km–300 km below the ICB. *Wen and Niu* [2002] analyzed global data and suggested a hemispherical pattern in the attenuation structure at the top of the inner core. (More recent global analyses include those of *Cormier and Li* [2002], *Li and Cormier* [2002], *Garcia et al.* [2006], and *Yu and Wen* [2006].) Considering that these authors analyze different depth ranges and geographical areas of the inner core, it is difficult to make a useful inference from these observations alone, and thus more thorough studies of the inner core attenuation are warranted. Here we extend and improve the analysis of *Kazama et al.* [2008] to construct a 1-D attenuation model of the top half of the inner core.

[3] *Kazama et al.* [2008] measured the attenuation parameter (t^*) from the amplitude ratio between PKP(DF)

and PKP(BC, AB). As this method can be applied only when core phases are well isolated in time, applicable events and epicentral distance ranges are very limited. *Chevrot* [2002] and *Garcia et al.* [2004] used simulated annealing (SA) to extract traveltimes, attenuations and other parameters by optimizing the fit between observed and modeled waveforms. This method should be applicable to waveform data with severe contaminations due to phase overlaps, and allows us to overcome the limitation mentioned above. In this study, we employ this method to extract attenuation parameters from core phases recorded by Japanese Hi-net. With an expanded data set, we obtain a well constrained 1-D attenuation model of the top 600 km of the inner core beneath the northeastern Pacific that shows a gradual increase of attenuation from the ICB to a depth of ~250 km followed by a gradual decrease, i.e., a high attenuation zone in the inner core.

2. Method of Analysis

[4] We modify the method of *Garcia et al.* [2004] slightly to achieve further flexibility for analyzing core phases of seismic array data. For an epicentral distance range where three core phases, PKP(DF), PKP(BC), and PKP(AB), are simultaneously observed, we assume that a waveform $S_i(t)$ at a station i can be modelled as

$$S_i(t) = R_i^{DF} A(t_i^{*DF}) * W(t + \tau_i^{DF}) + R_i^{BC} W(t + \tau_i^{BC}) + R_i^{AB} H * W(t + \tau_i^{AB}), \quad (1)$$

where $W(t)$ is a time series of a reference waveform common to all incoming core phases to the array; R_i^{DF} , R_i^{BC} and R_i^{AB} are amplitude corrections, that involve effects of the source radiation, geometrical spreading and transmission at boundaries, τ_i^{DF} , τ_i^{BC} and τ_i^{AB} are time delays from theoretical travel times, and H denotes the Hilbert transform operator; t_i^* is the differential attenuation parameters between PKP(DF) and the reference waveform, and $A(t^*)$ is an attenuation operator assuming a constant Q in the absorption band defined as

$$A(t^*) = \exp\left[-\frac{\omega t^*}{2} + i \frac{\omega t^*}{\pi} \log \frac{\omega}{\omega_0}\right] \quad (\omega_0 = 2\pi). \quad (2)$$

The only difference from the method by *Garcia et al.* [2004] is that the amplitude of PKP(BC), R_i^{BC} , is variable among stations so that data from a large aperture network such as Hi-net can be analyzed effectively.

[5] The distance range where three core phases are observed is only between 145–155 degrees, while PKP(DF) phases that traverse the inner core are observed between 110–180 degrees. To improve the resolution of the inner

¹Earthquake Research Institute, University of Tokyo, Tokyo, Japan.

Table 1. List of Events Analyzed in This Study

Event	Date	Time (GMT)	Latitude (deg)	Longitude (deg)	Depth (km)	Mw
1	29 June 2001	18:38:51	-19.47	-66.18	287.0	6.1
2	27 July 2003	11:41:28	-19.84	-64.94	350.6	6.0
3	17 March 2004	3:32:00	-21.24	-65.60	297.0	6.1
4	2 June 2005	10:55:58	-24.20	-66.86	191.0	6.1
5	26 July 2005	14:11:36	-15.41	-73.15	107.6	5.9
6	14 August 2005	2:39:39	-19.84	-69.27	117.1	5.8
7	18 Nov. 2007	5:40:17	-22.70	-60.50	261.7	6.0
8	12 Oct. 2008	20:55:44	-20.30	-65.23	361.5	6.2
9	30 Sep. 2009	19:03:00	-15.55	-69.29	255.4	5.8
10	18 June 2001	19:56:56	-24.29	-69.17	88.8	5.8
11	28 August 2001	6:56:09	-21.72	-70.11	65.6	5.8
12	16 July 2006	11:42:41	-28.71	-72.84	12.0	6.2
13	14 Nov. 2007	17:44:00	-23.22	-70.53	38.0	5.8
14	17 April 2009	2:08:08	-19.58	-70.48	25.0	6.1
15	17 Nov. 2005	19:38:00	-22.46	-68.13	155.3	6.8
16	25 August 2006	0:44:46	-24.44	-67.18	185.8	6.6

core, it is critical to utilize PKP(DF) waveforms with all observable distances. We therefore model PKP(DF) waveforms for distances beyond the C-cusp and distances in front of the B-cusp as

$$S_i(t) = R_i^{DF} A(t_i^{*DF}) * W(t + \tau_i^{DF}). \quad (3)$$

[6] The unknown parameters are thus t_i^* , R_i^{DF} , R_i^{BC} , R_i^{AB} , τ_i^{DF} , τ_i^{BC} , τ_i^{AB} , and $W(t)$ in (1), and t_i^* , R_i^{DF} , τ_i^{DF} and $W(t)$ in (3). $W(t)$ in (1) and (3) should be identical for a given earthquake. Although we can simultaneously determine all of the above parameters using the method of simulated annealing, for simplicity and saving of the required CPU time, we conduct a two-step optimization. First, using only data with three core phases, we determined the parameters in (1). Second, using the rest of data, we determined t_i^* , R_i^{DF} and τ_i^{DF} in (3) with fixing $W(t)$ to the optimal values obtained in the first step. Theoretical traveltimes of the three core phases are calculated for the VMOI model [Kaneshima *et al.*, 1994] which is our reference velocity model of the core beneath the northeastern Pacific.

[7] The waveform inversion is performed by minimizing the L1 norm misfit function of the difference between observed and model waveforms. The optimization scheme is essentially the same as that by *Chevrot* [2002] who uses the Metropolis algorithm of SA [e.g., *Sen and Stoffa*, 1995], and here we briefly summarize it. After extensive trial and error tests for full waveform synthetics, we chose the cooling schedule, $T_k = 0.99^k T_0$ [Iritani, 2010], where T_k is the temperature at the k th iteration, T_0 is the initial temperature which is set to three times of the initial L1 norm misfit function, and the total number of iteration is 2000. Initial values of parameters are set as $W(t) = 0$, $R = 0$, $\tau = 0$, and $t^* = 1$. One iteration at each temperature includes random perturbations for all of the four parameters. The reference waveform $W(t)$ is perturbed 1% of the maximum amplitude of the entire record section within a pre-established time window, and the perturbation is accepted only when the misfit function decreases. The length of the perturbed time window varies with events. (e.g., when analyzing shallow

events, we deal with overlapping problem of depth phases by extending the time window to include depth phases). Random perturbations to R , τ , t^* are given by:

$$R = 0.01n_R \quad (0 < R < 2)$$

$$\tau = n_\tau \Delta t \quad (-2s < \tau < 2s)$$

$$t^* = 0.01n_{t^*} \quad (0 < t^* < 1)$$

where n_R , n_τ and n_{t^*} are integral uniform random numbers such that the parameters stays in the specified ranges, and Δt is the sampling interval. The trade-off between the amplitude of the reference waveform and the amplitude correction term of the BC phase is overcome by fixing the maximum amplitude value of R_i^{BC} in each record section to 1, and the summation of the time delay of the BC phase $\sum \tau_i^{BC} = 0$ at each iteration to avoid their indeterminacy. This optimization problem is solved 20 times with different random seeds, and the average and standard deviation of the optimal values are regarded as the measured values and their errors.

3. Data Set

[8] We analyze the vertical component of core phases recorded by Hi-net. Waveforms with high S/N ratios for sixteen events with Mw greater than 5.8 occurred in the South American region between 2001 and 2009 are used (Table 1). PKP(DF) from this region to Japan take an “equatorial” path of the inner core beneath the northeastern Pacific (Figure 1a). Each trace is band-pass filtered with corner frequencies of 0.5 Hz and 1.5 Hz and normalized by the maximum amplitude. After obtaining optimal traveltimes (and other parameters) we discard data which appear to suffer from cycle skipping problems. *Garcia et al.* [2004, 2006] applied their method only to data in which 3 core phases exist. To improve resolution at shallower part of the inner core, we apply our method even to data in which only PKP(DF) are observed. Events #10–14 are shallow depth events (<100 km), for which source time functions become complex due to depth phases. The resultant number

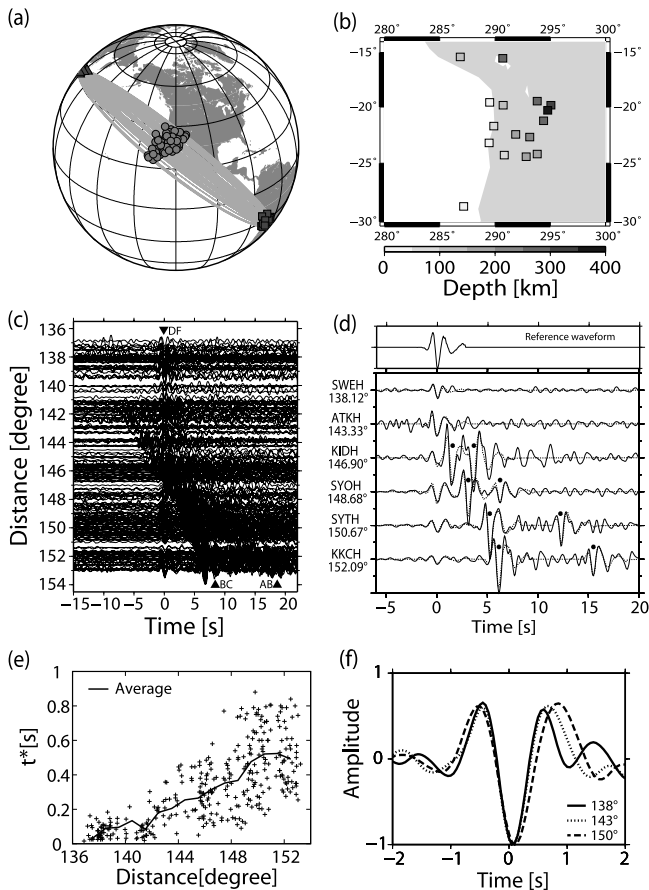


Figure 1. Ray paths and hypocenters, and an example of the analysis for event #5. (a) Examples of ray paths of PKP(DF). Hypocenters (solid square) and stations (solid triangles) are also shown. Gray circles denote the turning point. (b) The distribution of the events analyzed. (c) Observed seismograms. Waveforms are aligned by the measured traveltimes of PKP(DF). (d) (top) The derived reference waveform. (bottom) Comparison of the observed data (solid lines) and the modeled waveforms for the optimal parameters (dashed lines) for several typical traces. Closed circles denote measured traveltimes. (e) The measured attenuation parameters (plus) and their average for each epicentral distance bin with 1 degree width (solid line). (f) The comparison of stacked PKP(DF) phases belonging to 1-degree width bins. Each waveform is normalized by the maximum amplitude.

of traces in our data set is 4300, which is about five times larger compared with that of *Kazama et al.* [2008].

4. Results

[9] Figures 1c–1f show an example of our analysis for Event #5 for which the array distance coverage is from 137 degree to 153 degree corresponding to DF-phase bottoming depths of 40–320 km from the ICB. The estimated t^* in Figure 1e indicates a gradual increase with distance that can be visually confirmed from the broadening of waveforms with distance (Figure 1f). Although PKIKP precursors scattered around the CMB [e.g., *Shearer et al.*, 1998] are observed in the range between 142–145 degree, amplitudes

of these waves are small relative to DF phases and DF phases are distinctly separated from scattered waves at least for the range shorter than 144 degree. The scattered energy may contaminate the DF branch near the caustic between 144 to 146 degrees, but it is not evident both in waveforms and t^* estimates.

[10] The obtained attenuation parameters for this and other events show a consistent trend (Figure 2): the attenuation increases with distance from 136 to 150 degrees and

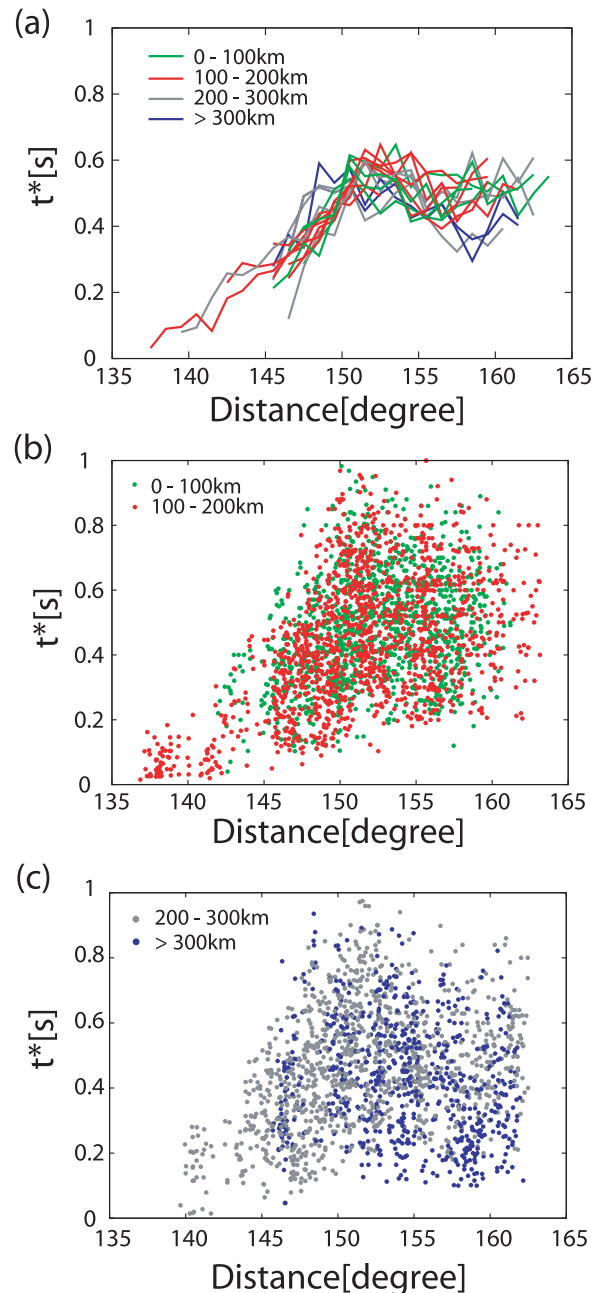


Figure 2. (a) Measured attenuation parameters for all events analyzed. The averages for each epicentral distance in 1-degree bins are plotted. Different color lines denote difference of the event depth. (b) Individual measurements for events shallower than 100 km (green) and between 100 km and 200 km (red). (c) For events between 200 km and 300 km (gray) and deeper than 300 km (blue).

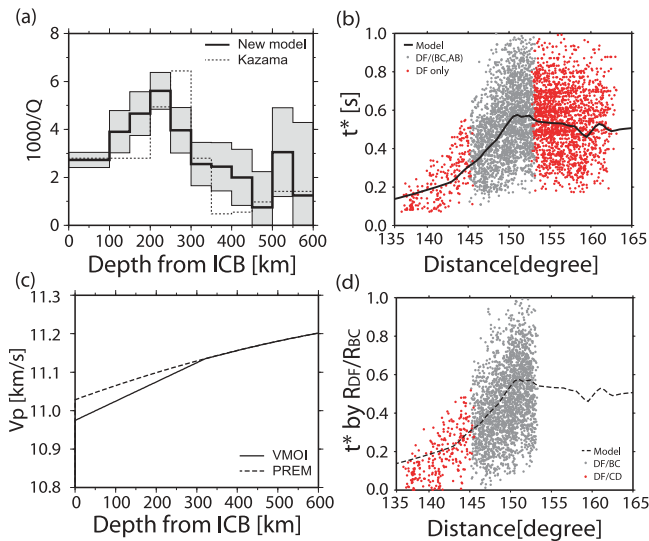


Figure 3. (a) The depth profile of the attenuation model. The model obtained by this study (solid line) and the model by *Kazama et al.* [2008] (dashed line) are compared. The estimated errors for our model are shown by shaded gray. (b) Comparison of individual attenuation parameter measurements (solid circle) and theoretical attenuation parameters predicted by the new model (black solid line). Red circles denote data points of the distance range where only DF phases are analyzed. Note that the general trend does not depend on the analysis method. (c) Velocity models of PREM and VMOI. (d) Similar to Figure 3b but t^* is estimated from amplitude ratio of R_i^{DF}/R_i^{BC} (grey circles) or R_i^{DF}/R_i^{CD} (red circles). Although there appears a slight bias, the general trend is quite consistent with that of Figure 3b. R_i^{CD} is an amplitude correction factor similarly defined as R_i^{BC} .

then slightly decreases. (Note that the distance here is defined as an distance of a DF ray if the source is at the Earth surface.) In Figure 2, we distinguish the results according to the event depth to investigate source side effects. As there is no systematic difference for different event depths, the source side effects seem small. Although there appears to exist a slightly different trend for the deep events (blue color), the deviation from the general trend is within the error bar of the data and does not alter the basic trend inferred here. The trend is also consistent with *Kazama et al.* [2008] who analyzed completely independent information of core phase, i.e., amplitude ratio. For these reasons, we conclude that the observed trend is likely due to the real 1-D inner core structure and not to heterogeneous structures in the vicinity of sources.

[11] Based on these observations, we invert for a 1-D attenuation model of the inner core by using the conventional least-square method. We define 11 layers in the top 600 km of the inner core: the top layer with 100 km thick and the other 10 layers with 50 km thick. For the actual inversion, we use individual t^* measurements corrected for the effect of the mantle attenuation as data (Figure 3b), and the correction, which is relatively minor considering the large scatter and uncertainty in individual t^* estimates, is made as follows. In our SA array analysis of core phases,

attenuation parameters are measured relative to a reference waveform $W(t)$ which is unique for each earthquake and estimated from the entire core phases within the distance range where three core phases are observed. Assuming the outer core attenuation is negligible, therefore, the ray path difference of three core phases affects our problem in two ways: (1) difference of mantle attenuation for AB and BC phases in estimating $W(t)$, and (2) difference of mantle attenuation between DF and BC. Tests using full-wave synthetic core phases indicate that $W(t)$ is more or less controlled by the average of the larger amplitude BC phases, and that (1) further introduces additional “broadening” in $W(t)$ estimate (relative to $W(t)$ estimated solely for BC phases) equivalent of a differential t^* value of ~ 0.03 . The effect of (2) can be estimated for a given attenuation model (PREM), by evaluating an average of the mantle attenuation for BC phases that affects the $W(t)$ estimate. The overall correction values are around 0.05.

[12] The inverted new attenuation model (Figure 3a) shows a moderate attenuation ($Q_p^{-1} \approx 1/370$) at the top of the inner core, a gradual increase down to a depth of 200–250 km where it has a peak of $Q_p^{-1} \approx 1/180$, and a decrease to a depth of 450–500 km below which the attenuation becomes insignificant. This result indicates that a high attenuation zone exists in around 250 km depth below the ICB. *Wen and Niu* [2002] analyzed PKP(CD) and PKP(DF) and suggested that Q_p^{-1} is around $1/600$ at the top of the inner core in the western hemisphere. Our model is generally consistent with their results and reveals a gradual increase of attenuation with depth. We also note that it is consistent with the three-layer attenuation model of *Garcia et al.* [2006], but with a better depth resolution.

5. Discussion

[13] The inner core attenuation of this study is measured, in essence, by estimating “pulse broadening” of each DF phase relative to the reference waveform $W(t)$ determined from the array data. Although it is a differential measurement in this sense, it differs from more conventional differential methods those directly compare core phases within each seismogram [e.g., *Doornbos, 1974; Kazama et al., 2008*], and thus it is possible that properties unique for individual stations are reflected into the attenuation measurements. To assure the robustness of our results, we have first confirmed that appreciable station static attenuation terms are absent. Secondly, the amplitude ratio of PKP(DF) to PKP(BC), R_i^{DF}/R_i^{BC} , after correction for known terms such as the source radiation, are converted to t^* by assuming that the peak amplitude of $A(t^*)$ in time domain can be approximated by $\exp(-\pi t^*)$ at 1 Hz. This assumption may introduce about 1–2% error in t^* estimate. Estimated t^* in Figure 3d shows a consistent trend as in Figure 3b, and confirms the robustness of our analysis based on SA.

[14] *Iritani* [2010] conducted a SA array analysis for broadband waveforms of event #11 recorded at stations in northeast China, and obtained similar results with those observed here (both attenuation and traveltimes). As the bottoming points of rays from the source to northeast China are beneath central Canada, the model obtained in this study is likely to represent the properties of a wider region of the inner core beneath the North America, and we suggest it may be representative of the western hemisphere (WH) of

the inner core (“equatorial” path) [Tanaka and Hamaguchi, 1997; Niu and Wen, 2001].

[15] We note that the seismic velocity of the shallow part of the inner core of the WH is low compared to PREM [Kaneshima et al., 1994; Wen and Niu, 2002]. Our reference velocity model VOMI [Kaneshima et al., 1994], which explains the basic trend of our traveltimes observations, indeed shows a gradual increase of V_p relative to PREM from top to a depth of ~ 300 km where it becomes indistinguishable from PREM (Figure 3c). This coincidence of the gradual increase of both V_p and attenuation from the surface to a depth of ~ 250 – 300 km in the WH may reflect a growth process of the inner core. Based on laboratory experiments for convection in the outer core driven by a thermally heterogeneous mantle, Sumita and Olson [1999] suggested that the hemispheric variation in inner core properties is consistent with differential crystallization rates, although there is disagreement on the relative rates [Aubert et al., 2008]. The gradual change with depth may also reflect a texture change with depth due to some convection motion occurring there [e.g., Cormier, 2007]. It is also possible that the depth dependence of the attenuation is due to a shift of the absorption band with depth [e.g., Doornbos, 1983; Li and Cormier, 2002]. As our measurement is band limited around 1 Hz, a further analysis of broadband data is warranted to find out whether or not frequency dependence of Q^{-1} is required from data.

[16] The presence of the attenuation peak at a depth of 200–250 km and the gradual decrease of attenuation below is also an interesting observation that should be resolved in the future.

[17] **Acknowledgments.** We thank K. Shiomi, M. Matsubara and the staff of Hi-net data center for providing us with the waveform data. We also thank T. Kazama for the general help on the data analysis, and S. Tanaka and G. Helffrich for discussion. Comments on the manuscript by G. Helffrich and two anonymous referees improved the manuscript. The Generic Mapping Tools [Wessel and Smith, 1998] is used to draw some of the figures. This work is partly supported by Grant-in-Aid for Scientific Research 19104011.

References

- Aubert, J., H. Amit, G. Hulot, and P. Olson (2008), Thermo-chemical wind flows couple Earth’s inner core growth to mantle heterogeneity, *Nature*, 454, 758–761.

- Chevrot, S. (2002), Optimal waveform and delay time analysis by simulated annealing, *Geophys. J. Int.*, 151, 164–171.
- Cormier, V. (2007), Texture of the uppermost inner core from forward and back scattered seismic waves, *Earth Planet. Sci. Lett.*, 258, 442–453.
- Cormier, V. F., and X. Li (2002), Frequency-dependent seismic attenuation in the inner core: 2. A scattering and fabric interpretation, *J. Geophys. Res.*, 107(B12), 2362, doi:10.1029/2002JB001796.
- Doornbos, D. J. (1974), The anelasticity of the inner core, *Geophys. J. R. Astron. Soc.*, 38, 397–415.
- Doornbos, D. J. (1983), Observable effects of the seismic absorption band in the Earth, *Geophys. J. R. Astron. Soc.*, 75, 693–711.
- Garcia, R., S. Chevrot, and M. Weber (2004), Nonlinear waveform and delay time analysis of triplicated core phases, *J. Geophys. Res.*, 109, B01306, doi:10.1029/2003JB002429.
- Garcia, R., H. Tkalcic, and S. Chevrot (2006), A new global PKP data set to study the Earth’s core and deep mantle, *Phys. Earth Planet. Inter.*, 159, 15–31.
- Iritani, R. (2010), Analysis of core phases using simulated annealing (in Japanese), M.S. thesis, 70 pp., Univ. of Tokyo, Tokyo.
- Kaneshima, S., K. Hirahara, T. Ohtaki, and Y. Yoshida (1994), Seismic structure near the inner core–outer core boundary, *Geophys. Res. Lett.*, 21, 157–160.
- Kazama, T., H. Kawakatsu, and N. Takeuchi (2008), Depth-dependent attenuation structure of the inner core inferred from short-period Hi-net data, *Phys. Earth Planet. Inter.*, 167, 155–160.
- Li, X., and V. F. Cormier (2002), Frequency-dependent seismic attenuation in the inner core: 1. A viscoelastic interpretation, *J. Geophys. Res.*, 107(B12), 2361, doi:10.1029/2002JB001795.
- Niu, F., and L. Wen (2001), Hemispherical variations in seismic velocity at the top of the Earth’s inner core, *Nature*, 410, 1081–1084.
- Sen, M., and P. Stoffa (1995), *Global Optimization Methods in Geophysical Inversion*, Elsevier Sci., New York.
- Shearer, P. M., M. A. H. Hedlin, and P. S. Earle (1998), PKP and PKKP precursor observations: Implications for the small-scale structure of the deep mantle and core, in *The Core-Mantle Boundary Region, AGU Geodyn. Ser.*, vol. 28, edited by M. Gurnis et al., pp. 37–55, AGU, Washington, D. C.
- Sumita, I., and P. Olson (1999), A laboratory model for convection in Earth’s core driven by a thermally heterogeneous mantle, *Science*, 286, 1547–1549.
- Tanaka, S., and H. Hamaguchi (1997), Degree one heterogeneity and hemispherical variation of anisotropy in the inner core from PKP(BC)–PKP(DF) times, *J. Geophys. Res.*, 102, 2925–2938.
- Wen, L., and F. Niu (2002), Seismic velocity and attenuation structures in the top of the Earth’s inner core, *J. Geophys. Res.*, 107(B11), 2273, doi:10.1029/2001JB000170.
- Wessel, P., and W. H. F. Smith (1998), New, improved version of the Generic Mapping Tools released, *Eos Trans. AGU*, 79, 579.
- Yu, W.-C., and L. Wen (2006), Inner core attenuation anisotropy, *Earth Planet. Sci. Lett.*, 245, 581–594.

H. Kawakatsu, R. Iritani, and N. Takeuchi, Earthquake Research Institute, University of Tokyo, 1-1-1 Yayoi, Bunkyo-ku, Tokyo 113-0032, Japan. (ryohei9@eri.u-tokyo.ac.jp)